Check for updates

ADVANCED HEALTHCARE MATERIALS
www.advhealthmat.de

Neutrophil Cyto-Pharmaceuticals Suppressing Tumor Metastasis via Inhibiting Hypoxia-Inducible Factor-1α in Circulating Breast Cancer Cells

Ying Zhang, Cong Wang, Weishuo Li, Wei Tian, Chunming Tang, Lingjing Xue, Ziming Lin, Guilai Liu, Dongfei Liu, Ying Zhou, Qianqian Wang, Xu Wang, Lutz Birnbaumer, Yong Yang, Xianjing Li, Caoyun Ju,* and Can Zhang**

Circulating tumor cells (CTCs) are reported as the precursor of tumor metastases, implying that stifling CTCs would be beneficial for metastasis prevention. However, challenges remain for the application of therapies that aim at CTCs due to lack of effective CTC-targeting strategy and sensitive therapeutic agents. Herein, a general CTC-intervention strategy based on neutrophil cyto-pharmaceuticals is proposed for suppressing CTC colonization and metastasis formation. Breast cancer 4T1 cells are infused as the mimic CTCs, and 4T1 cells trapped are first elucidated in neutrophil extracellular traps (NETs) expressing high levels of hypoxia-inducible factor-1α (HIF-1α) due to NET formation and thus promoting tumor cell colonization through enhanced migration, invasion and stemness. After verifying HIF-1α as a potential target for metastasis prevention, living neutrophil cyto-pharmaceuticals (CytPNEs) loaded with HIF-1α inhibitor are fabricated to therapeutically inhibit HIF-1α. It is demonstrated that CytPNEs can specially convey the HIF-1α inhibitor to 4T1 cells according to the inflammatory chemotaxis of neutrophils and down-regulate HIF-1α, thereby inhibiting metastasis and prolonging the median survival of mice bearing breast cancer lung metastasis. The research offers a new perspective for understanding the mechanism of CTC colonization, and puts forward the strategy of targeted intervention of CTCs as a meaningful treatment for tumor metastasis.

1. Introduction

Metastasis is one of the main causes of cancer deaths, and acts as the greatest challenge faced by malignancy therapy in the clinic. The metastases originate mainly from tumor cells departed from the primary tumor into blood, known as circulating tumor cells (CTCs). Subsequently, the CTCs survived from the shear stress and immune recognition, disseminate to distal organs followed by colonization and proliferation, eventually forming tumor metastases.[1] That is, CTCs are responsible for the formation of new distant metastases.[2] Apparently, if the CTCs can be stifled on its half way, such as eliminating CTCs in the bloodstream[3] or inhibiting their colonization at distal organ,[4] the metastasis cascade would be interrupted, aiding metastasis prevention.

Challenges remain for the application of therapies that aim at CTCs. First, it is difficult to recognize and deliver drugs to the CTCs which are rare infrequent in the bloodstream, about average 1 CTC per 1 billion peripheral blood cells.[5] Despite specific ligands such as anti-epithelial cell

Y. Zhang, C. Wang, W. Li, C. Tang, L. Xue, Z. Lin, Y. Zhou, Q. Wang, C. Ju, C. Zhang
State Key Laboratory of Natural Medicines
Center of Advanced Pharmaceuticals and Biomaterials
China Pharmaceutical University
Nanjing 210009, P. R. China
E-mail: jucaoyun@cpu.edu.cn; zhangcan@cpu.edu.cn

W. Tian, G. Liu, X. Wang, Y. Yang, X. Li
State Key Laboratory of Natural Medicines
Center for New Drug Safety Evaluation and Research
China Pharmaceutical University
Nanjing 210009, P. R. China
E-mail: xjl@cpu.edu.cn

D. Liu
School of Pharmacy
China Pharmaceutical University
Nanjing 210009, P. R. China

L. Birnbaumer
Neurobiology Laboratory
National Institute of Environmental Health Sciences
Research Triangle Park, NC 27709, USA

L. Birnbaumer
Institue of Biomedical Research (BIOMED)
School of Medical Sciences
Catholic University of Argentina
Buenos Aires C1107AFF, Argentina

The ORCID identification number(s) for the author(s) of this article can be found under https://doi.org/10.1002/adhm.202101761

DOI: 10.1002/adhm.202101761

 © 2021 Wiley-VCH GmbH

adhesion molecule (EpCAM) have been developed to capture the antigen-expressing CTCs, CTCs may dynamically vary the expression of a given antigen under certain conditions,[6] resulting in insufficient targeting ability. Moreover, CTCs from varied primary tumors possess respective specific antigen.[6] Namely, different cancer types might require varied CTC-targeting strategies, which makes this targeting approach more intricacy. Therefore, a general and efficient CTC-targeting strategy is in great desire. Second, although the existence of CTCs has been known for decades, the biological mechanisms behind their super metastatic ability are only partially understood.[7] Of note, there still lacks of sensitive drugs against CTCs to date. For this reason, exploring the crucial signaling pathways commonly involved in various cancer types to blunt their metastatic ability are in urgent need, which might provide novel therapeutic agents against CTCs.

Hypoxia is highly associated with tumor progression and metastasis, leading to the enhanced expression and activity of hypoxia inducible factor-1α (HIF-1α). HIF-1α involves in every step of the metastatic process, including regulating angiogenesis, extracellular matrix remodeling, motility and immune evasion.[8] These observations of HIF-1α mainly focused on the primary tumors, while the HIF-1α associated downstream consequences in CTCs has been rarely explored. Of note, a clinical study has found the high accumulation of HIF-1α in CTCs of breast cancer patients,[9] which suggests a probably relationship between HIF-1α and CTC metastasis. Additionally, emerging evidence shows in circulation of triple negative breast cancer patients, neutrophils, the most abundant type of immune cells, can be activated by CTCs to extrude its chromatin and granule proteins to form an extracellular fibril matrix, namely neutrophil extracellular traps (NETs).[10] Further, NETs are liable to trap the CTCs, forming CTC-NET clusters, as observed around metastatic foci in human triple negative breast cancer with a poor prognosis,[10,11] With cytokines release, more neutrophils are recruited to the CTC-NET clusters.[12] Notably, reactive oxygen species (ROS)-producing respiratory burst, accompanying the NET formation,[13] has the potential to inhibit the activity of proline hydroxylases (PHDs) for degradation of HIF-1α in tumor cells,[14] and leads to the accumulation of HIF-1α.[15] Therefore, considering the high level of HIF-1α in CTCs and the existence of CTC-NET clusters within enhanced ROS level, we hypothesized that HIF-1α in CTCs trapped by NETs might also be a crucial signal in tuning CTC metastatic ability, and targeted inhibiting the HIF-1α in CTCs would suppress the metastasis. As far as we know, it is the first time that the role of HIF-1α in promoting CTC metastasis was explored and this CTC-intervention strategy has been come up with.

Herein, breast cancer 4T1 cells were utilized to mimic the CTCs in this study due to the hard-to-get of CTCs that are rare in the blood. We first verified the high HIF-1α level in circulating breast cancer cells trapped in NETs, as well as its contribution to the high metastatic capacities, including migration, invasion, immune escape and stemness. After understanding the role of HIF-1α in CTC-NET clusters to enhance metastasis, we proposed a novel targeted-intervention strategy using the inflammatory chemotaxis of neutrophils to the local pro-inflammatory microenvironment of CTC-NET clusters[12] for the delivery of HIF-1α inhibitor, BAY 87–2243[16] (hereafter referred to BAY). A living neutrophil cyto-pharmaceutical of BAY (CytPNEs) was fabricated on the basis of our previous works.[17] After injection, CytPNEs precisely delivered BAY into circulating 4T1 tumor cells and profoundly inhibited HIF-1α, thus suppressing the formation of metastatic foci and significantly prolonging the survival time of mice bearing breast cancer lung metastasis (**Figure 1**). Meanwhile, the mechanism of colonization of CTCs that followed the intervention of HIF-1α in the clusters could be explored. This study provides brand-new insights into the mechanism of CTC colonization, and puts forward the strategy of targeted intervention of CTCs as a meaningful treatment for tumor metastasis.

2. Results

2.1. High Abundance of HIF-1α in NET Trapped CTCs

To better understand the existence of CTCs trapped in NETs at circulation in highly metastatic breast cancer, we first established the breast cancer lung metastasis in mice by an intravenous injection of mCherry-expressing 4T1 cells (mCherry-4T1 cells, 10^6 cells per mouse). At 24 h post-injection, the lung tissues were collected and examined by immunofluorescence. In the lumen of the pulmonary capillaries (**Figure 2**a), we observed that mCherry-4T1 cells (Red) were surrounded by large amounts of neutrophil elastase (Green), a typical marker of NETs, which was also observed by other group.[18] Further, we used citrullinated histone H3 (H3Cit) to indicate the NET production and found the high abundance of HIF-1α in CTCs trapped in NETs in the lung sections as evidenced by the bright green fluorescence of HIF-1α located in red 4T1 cells (Figure 2b). By contrast, the 4T1 tumor cells that were not trapped in NETs displayed decreased level of HIF-1α (Figures S1 and S2, Supporting Information). These results confirmed the high level of HIF-1α in NET trapped CTCs in vivo.

Next, we mimicked the process of NETs trapping CTCs in vitro for detailed investigation.[19] To begin with, NETs were induced by the stimulation of neutrophils with phorbol 12-myristate 13-acetate (PMA, a strong stimulator of NET formation[20]), which resulted in increased adhesion to 4T1 cells compared with unstimulated neutrophils (Figure S3, Supporting Information). Then, NETs were co-incubated with mCherry-4T1 cells to form the "4T1-NET clusters". As presented in Figure 2c, the discrete mCherry-4T1 cell (Red) was trapped by neutrophil elastase (Green) and filamentous DNA (Blue). We further confirmed the successful establishment of CTC-NET structure-filamentous NETs encircling the tumor cells-in vitro by scanning electron microscopy (Figure 2d).

The HIF-1α level in the mCherry-4T1 cells trapped in NETs was also detected (Figure 2e). Cobalt chloride ($CoCl_2$), a chemical inhibitor of prolyl hydroxylases,[21] was applied to co-culture with mCherry-4T1 cells to yield an intracellular hypoxia (positive control). As expected, an abundance of HIF-1α (Green) in mCherry-4T1 cells of 4T1-NET clusters was observed, whereas the green fluorescence of HIF-1α was barely seen in discrete mCherry-4T1 cells under normoxia. Moreover, treatment with DNase-for degradation of NETs or BAY-for pharmacologic inhibition of HIF-1α accumulation significantly suppressed the accumulation of HIF-1α in the 4T1 cells trapped in NETs, further demonstrating the crucial role of NETs in HIF-1α accumulation in CTCs. Similarly,

© 2021 Wiley-VCH GmbH

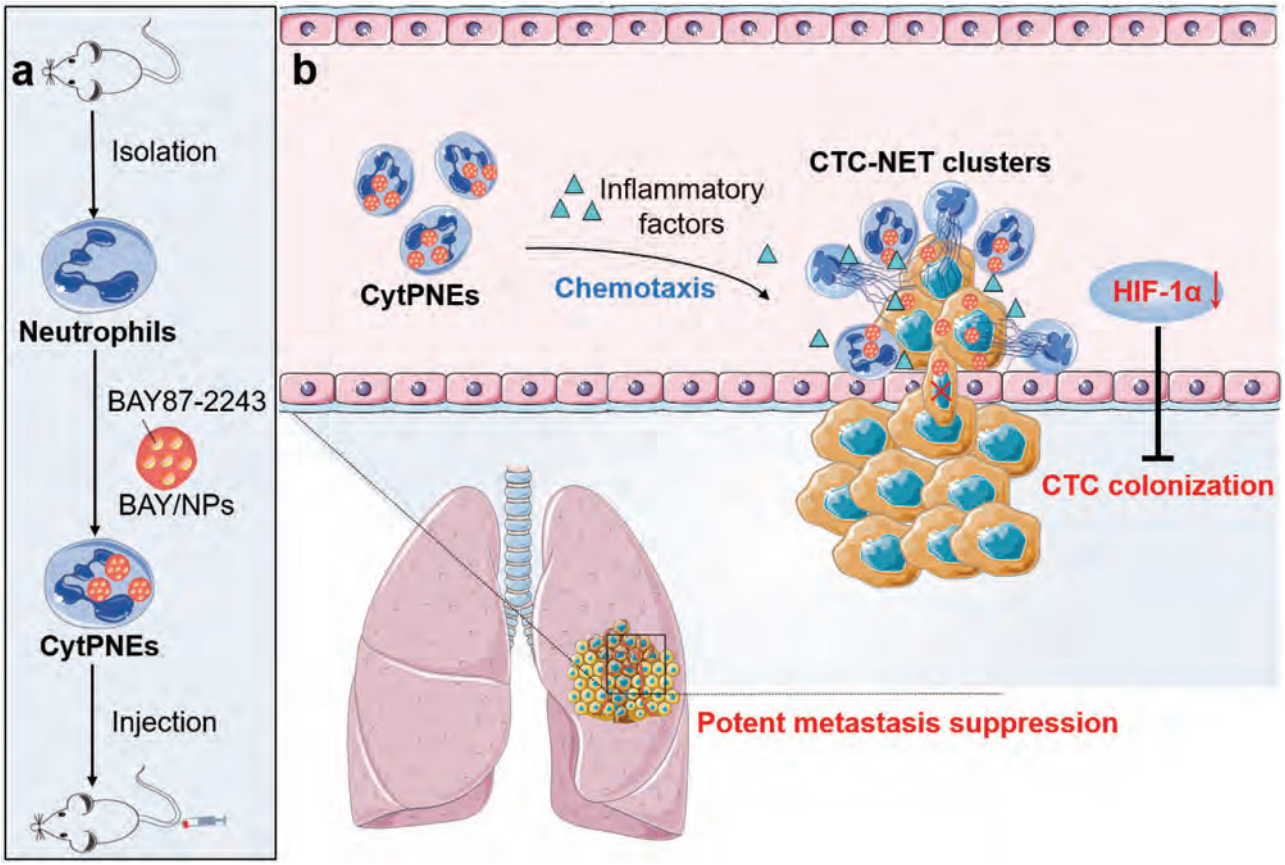

Figure 1. Schematic design of a CTC-intervention neutrophil cytopharmaceutical (CytPNEs) for inhibition of tumor metastasis. a) Schematic illustration of the preparation of CytPNEs. b) Schematic illustration shows that CytPNEs can be effectively recruited to the CTCs trapped in the NETs (CTC-NET clusters) due to the inflammatory chemotaxis, followed by down-regulating the HIF-1α level in CTCs, and finally reduce the formation of tumor metastasis through suppressing CTC colonization and metastasis formation.

the HIF-1α protein in 4T1 cells trapped in NETs analyzed by western blot exhibited a significantly higher expression compared to that of discrete 4T1 cells or 4T1-NET clusters treated with DNase or BAY (Figure 2f,g).

Since HIF-1α under normoxia degrades rapidly,[22] we wondered why CTCs trapped in NETs exhibited a high level of HIF-1α at circulation. We first explored the resumption of HIF-1α in CTCs with the aid of NETs. 4T1 cells were initially incubated under hypoxia for 24 h followed by another incubation under normoxia for 2 h to mimic the oxygen tension confronted by CTCs.[23] Subsequently, the PMA-triggered NETs were utilized to trap 4T1 cells at normoxia condition for simulation of the CTC-NET clusters at circulation. The levels of HIF-1α in 4T1 cells were detected at different stages by western blot (Figure S4, Supporting Information). As expected, the hypoxia improved the HIF-1α accumulation in tumor cells, while it rapidly eliminated due to the oxygen-stimuli HIF-1α degradation. Notably, 4T1 cells recovered the HIF-1α abundance under normal oxygen environment by the aid of NET trapping, further confirming the central role of NET formation in aiding HIF-1α accumulation. After that, we explored the detailed mechanism of HIF-1α resumption by the assistance of NETs. As is known, an abundant of ROS can be released due to the respiratory burst of neutrophils accompanying with the NET formation.[24] More than this, ROS has been considered as an inhibitor of PHD, which can inhibit the activity of PHD and thereby restrain the degradation of HIF-1α.[25] Thus, the levels of ROS in the 4T1-NET clusters were assessed (Figure 2h and Figure S5, Supporting Information). Compared to the 4T1 cells alone, the ROS level was greatly increased in 4T1-NET clusters, which was mainly ascribed to the NET formation. This was further verified by the addition of DNase that degraded the formed NETs and thus reduced the local concentration of ROS production. Therefore, we concluded that a large amount of ROS released during the NET formation elevated the HIF-1α level, resulting in the accumulation of HIF-1α in NET trapped CTCs.

Taken together, our results confirmed that HIF-1α showed a high abundance in NET trapped CTCs, which was probably ascribed to the formation of NETs.

2.2. CTCs with High Accumulation of HIF-1α Displayed a Highly Metastatic Phenotype

HIF-1α has been closely linked to the high metastasis.[26] To verify the role of HIF-1α expressing CTCs in cancer metastasis, we first explored the migration of 4T1 cells trapped in NETs by transwell assay. The formed NETs significantly increased the migration of 4T1 cells of about 5-fold in comparison with 4T1 cells

© 2021 Wiley-VCH GmbH

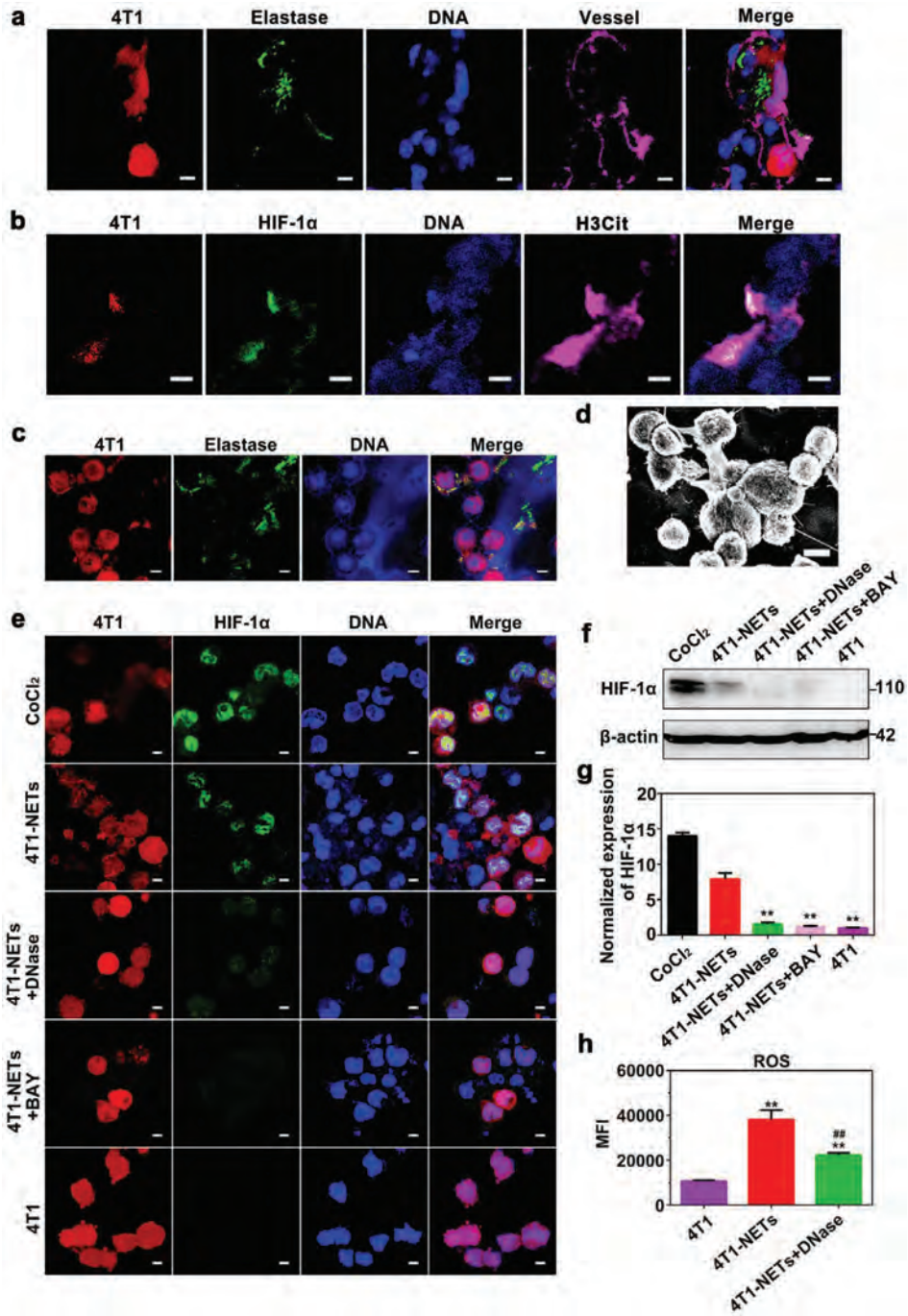

Figure 2. High abundance of HIF-1α in NET trapped CTCs. a) NET trapped CTCs were observed in the vicinity of the pulmonary capillaries. Circulating 4T1 tumor cells (Red) were surrounded by NETs that were accompanied with the neutrophil elastase stained by anti-neutrophil elastase antibody (Green). The nuclei and filamentous DNA were stained by DAPI (Blue), the vessels were labeled with CD31 antibody (Rose red). Scale bars: 5 µm. b) Circulating 4T1 tumor cells (Red) were surrounded by NETs that were accompanied with the citrullinated histone H3 (H3Cit) (Rose red). HIF-1α (Green) in the NET trapped CTCs was evaluated by immunofluorescence. Scale bars: 5 µm. c) Immunofluorescence of 4T1-NET clusters in vitro. Neutrophil elastase secreted by neutrophils localized to the NETs, which was stained by anti-neutrophil elastase antibody (Green) and surrounded the mCherry-4T1 cells (Red). The nuclei and filamentous DNA were stained by Hoechst 33 342 (Blue). Scale bars: 5 µm. d) Representative scanning electron microscope image of 4T1-NET clusters. Scale bars: 5 µm. e) Immunofluorescence of HIF-1α (Green) in NETs trapped 4T1 cells in vitro. $CoCl_2$-treated 4T1 cells were used as positive control and native 4T1 cells were used as negative control. Scale bars: 5 µm. f,g) The level of HIF-1α in the NETs trapped 4T1 cells was examined by western blot. Representative gel electrophoresis bands were shown (f), and the levels of the proteins were quantified by densitometry and normalized to the expression of β-actin (g). Densitometry data were shown as mean ± SEM, from $n = 3$ independent experiments. $^{**}P < 0.01$ versus 4T1-NETs. h) ROS level as determined by flow cytometry. Data were shown as mean ± SEM, from $n = 3$ independent experiments. $^{**}P < 0.01$ versus 4T1, $^{\#\#}P < 0.01$ versus 4T1-NETs.

© 2021 Wiley-VCH GmbH

alone (Figure S6, Supporting Information). Moreover, the invasiveness assay of 4T1 cells was detected on the human umbilical vein endothelial cell (HUVEC) monolayers. When 4T1 cells were trapped in NETs, the invasion of 4T1 cells exhibited 7-fold higher than 4T1 cells alone (**Figure 3**a and Figure S6, Supporting Information). In contrast, destructing the NETs by DNase, inhibiting the HIF-1α abundance by BAY, or knocking down the HIF-1α (4T1$^{\text{HIF-1}\alpha\text{-KD}}$ cells; Figure S7, Supporting Information) all restrained the migration and invasion ability of 4T1 cells trapped in NETs. These results indicated that the high level of HIF-1α in 4T1 cells by NETs formation promoted the migration and invasiveness of tumor cells, which was beneficial for tumor metastasis.[27]

Immune escape and stemness maintenance are the prerequisites for CTCs to colonize at distant organs.[28] We thereby explored the expression of immune checkpoint programmed cell death protein 1 ligand (PD-L1) for T cells,[29] and certain stemness- and proliferation-associated transcription factors including Nanog and Oct4.[28b] As shown in Figure 3b and Figure S8 (Supporting Information), 4T1 cells in 4T1-NET clusters exhibited a higher expression of PD-L1 compared with 4T1 cells alone. By contrast, the expressions of PD-L1 in the clusters receiving free BAY or HIF-1α knockdown were significantly down-regulated. These results suggested that the abundance of HIF-1α increased the potential of immune escape from T cells via inducing the PD-L1 expression. Similarly, the expressions of Nanog and Oct4 were both up-regulated in the 4T1-NET clusters compared with 4T1 cells alone (Figure 3c and Figure S9, Supporting Information), while their expressions were strikingly suppressed after a treatment of DNase or BAY. Additionally, almost no expression of Nanog and Oct4 was observed in 4T1$^{\text{HIF-1}\alpha\text{-KD}}$ cells, suggesting a positive relationship of stemness and HIF-1α abundance of CTCs. Therefore, we deduced that the HIF-1α in 4T1 cells trapped by NETs maintained the potent metastatic potential of tumor cells, including promoted migration, invasion, immune escape and stemness.

In order to further confirm the role of HIF-1α in maintaining the high metastatic phenotype of CTCs in vivo, we detected the lung metastases and the survival of mice bearing 4T1 lung metastasis (Figure 3d–f). As controls, DNase (2.5 mg kg^{-1}) was intramuscularly injected to destroy the formed NETs[19] (Figure S10, Supporting Information), and 4T1$^{\text{HIF-1}\alpha\text{-KD}}$ cells were applied instead of wild type 4T1 cells. The results showed that mice receiving wild type 4T1 cells exhibited the most metastatic nodules-about 38 per lung and no mice survived longer than 20 d. In a stark contrast, co-administration of DNase or injection of 4T1$^{\text{HIF-1}\alpha\text{-KD}}$ cells both significantly inhibited the formation of lung metastases and prolonged the survival time of 4T1-bearing mice. The H&E staining of lung sections of mice also demonstrated that destroying the NETs with DNase or knocking down HIF-1α in the 4T1 cells could significantly inhibit the metastatic nodules formation in lungs (Figure 3d,e). The Ki67 expression of lung sections also indicated that destroying the NETs with DNase or knocking down HIF-1α in 4T1 cells slowed down the proliferation efficiency of tumor cells, leading to the reduction of the CTCs colonization and metastasis formation (Figure 3d). Additionally, we evaluated the proportion of PD-1$^+$ or Tim3$^+$ CD8$^+$ exhausted T cells as well as the PD-L1 expression in metastatic site, which reflected the immune escape of CTCs at least to some extent (Figure 3g,h and Figure S11, Supporting Information). We showed that mice with wild type 4T1 cells infusion possessed the highest proportion of PD-1$^+$ or Tim3$^+$ CD8$^+$ exhausted T cells and PD-L1 expression, whereas destroying the NETs by DNase or knocking down HIF-1α in tumor cells both significantly decreased the PD-L1 expression in tumor cells and the related proportion of PD-1$^+$ or Tim3$^+$ CD8$^+$ exhausted T cells in the metastases.

Collectively, we believed that the high level of HIF-1α in CTCs trapped in NETs played functional roles in maintaining the highly metastatic phenotype of CTCs, which suggested HIF-1α in CTCs as a potential target for metastasis prevention.

2.3. Preparation and Characterization of BAY/NPs and CytPNEs

Since the high level of HIF-1α in CTCs involved in the multi-process of breast cancer lung metastasis, it could be a potential target for metastasis treatment. To validate our idea, we proposed a novel CTC-intervention strategy for the treatment of 4T1 lung metastasis by specially inhibiting the HIF-1α in CTCs trapped in NETs.

Leveraging the chemotaxis of neutrophils to the inflammatory microenvironment,[30] 4T1-NET clusters in this case (**Figure 4**a,b and Figures S12 and S13, Supporting Information), we fabricated living neutrophil cyto-pharmaceuticals on the basis of their endocytosis ability. To avoid the undesired effect of BAY on neutrophils, we first prepared BAY-loaded acetylated-dextran (Ac-DEX) nanoparticles (hereafter referred to BAY/NPs) for NE encapsulation. The diameter of BAY/NPs was about 240 nm (Figure 4c), with a uniformly spherical morphology as observed by transmission electron microscopy (Figure 4d). Then, according to our previous studies,[17] neutrophils were incubated with the BAY/NPs to afford the NE cyto-pharmaceuticals (CytPNEs) with 4.3 μg BAY per 10^6 neutrophils. Cell viability of CytPNEs was quantified using CCK-8 assays, which was more than 80% within 4 h (Figure 4e).

In addition, we evaluated the stability of CytPNEs in the transport process. CytPNEs were incubated with different culture media, including RPMI medium as normal physiological condition, RPMI medium with N-formyl-L-methionyl-L-leucyl-L-phenylalanine tripeptide (fMLP, a typical chemokine, 10×10^{-9} M) as chemotactic stimulus, and RPMI medium with PMA (a simulated inflammatory factor, 100×10^{-9} M) as inflammatory microenvironment, respectively. These results showed that CytPNEs were stable and without drug burst release under physiological condition (Figure 4f) and during the chemokine chemotaxis process (Figure 4g). While, CytPNEs rapidly released the loaded drug when located in the inflammatory microenvironment mimicked by PMA (Figure 4h). This was further confirmed by quantifying the fluorescence intensity of Coumarin 6 (C6, a fluorescent model drug) released from and retained in CytPNEs (Figure S14, Supporting Information).

2.4. CytPNEs Specially Delivered BAY to NET Trapped CTCs and Interfered with the HIF-1α Level in CTCs

We have shown that fresh neutrophils could effectively target the circulating 4T1 tumor cells trapped in NETs (Figure 4a,b), then we wondered whether CytPNEs loaded with HIF-1α inhibitor

© 2021 Wiley-VCH GmbH

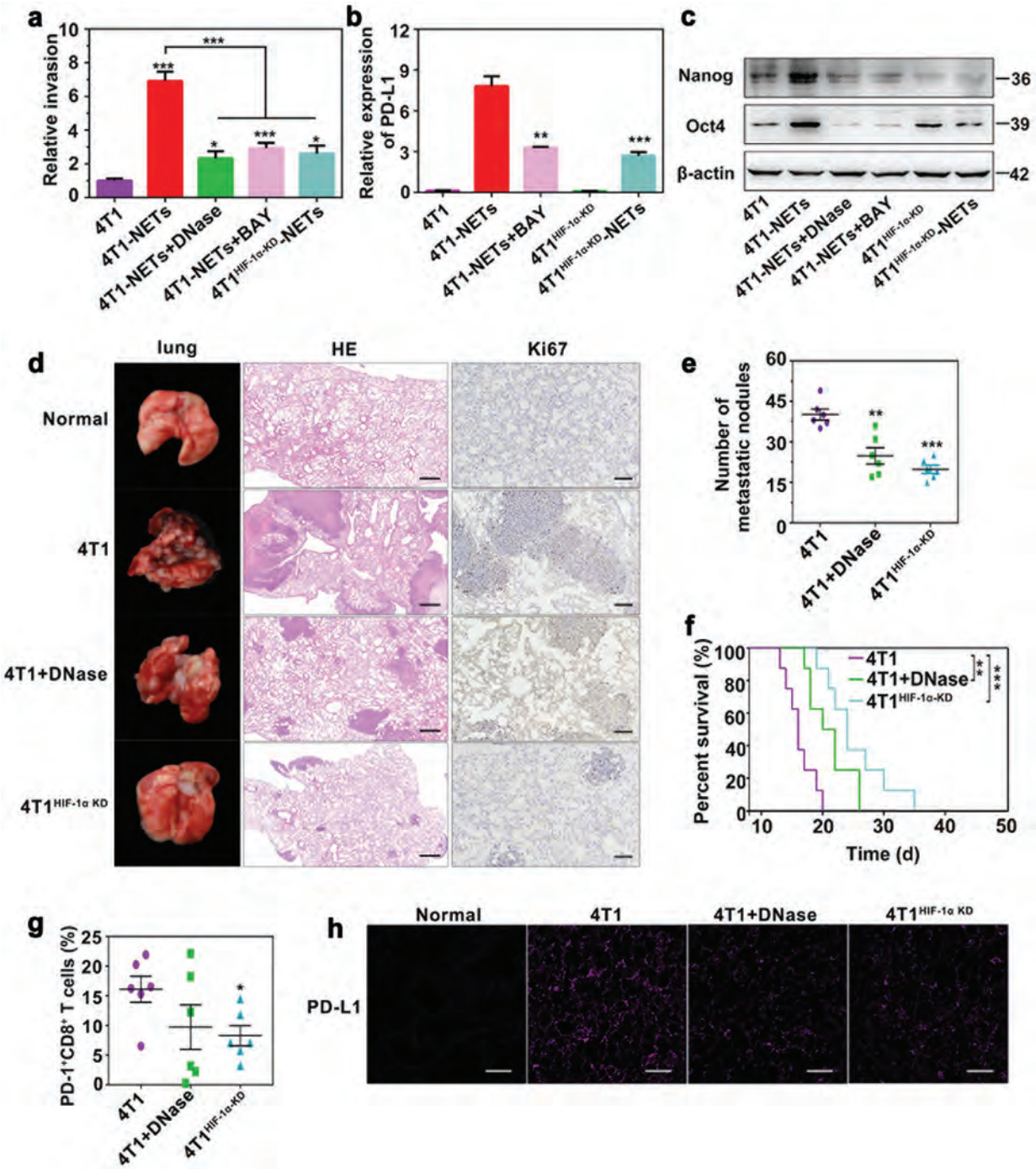

Figure 3. HIF-1α expressing CTCs displayed a highly metastatic phenotype. a) Invasion of 4T1 cells was determined using transwell assay. All other groups were normalized to the 4T1 group. (Mean ± SEM, from $n = 3$ independent experiments) * $P < 0.05$, *** $P < 0.001$ versus 4T1 cells alone. b) Expression levels of PD-L1 in 4T1 cells were measured by flow cytometry. Data were shown as mean ± SEM, from $n = 3$ independent experiments. ** $P < 0.01$, *** $P < 0.001$ versus 4T1-NETs. c) Expression levels of Nanog and Oct4 in 4T1 cells were determined by western blot. Representative gel electrophoresis bands were shown. d) Typical images of lung tissues, H&E and Ki67 stained lung sections harvested from healthy mice and mice injected with saline (normal), 4T1 cells (4T1), 4T1 cells and DNase (4T1+DNase), and $4T1^{HIF-1\alpha-KD}$ cells ($4T1^{HIF-1\alpha-KD}$). Scale bars: 500 µm (H&E), 100 µm (Ki67). Each mouse received 1×10^6 cells (i.v.). e) The number of visually detected metastatic nodules in lungs was counted in each group (Mean ± SEM; $n = 6$ samples per group), ** $P < 0.01$, *** $P < 0.001$ versus 4T1. f) Survival percentages of mice treated with 4T1 cells, 4T1+DNase and $4T1^{HIF-1\alpha-KD}$ cells ($n = 8$ per group). ** $P < 0.01$, *** $P < 0.001$ versus 4T1 cells. g) The proportion of PD-1$^+$ CD8$^+$ T cells in lung tissues harvested from 4T1, 4T1+DNase and $4T1^{HIF-1\alpha-KD}$ treated mice (Mean ± SEM; $n = 6$ samples per group). * $P < 0.05$ versus 4T1 cells. h) Immunofluorescence of PD-L1 (Rose red) in lung sections harvested from healthy mice and mice treated with saline (normal), 4T1 cells (4T1), 4T1 cells and DNase (4T1+DNase), and $4T1^{HIF-1\alpha-KD}$ cells ($4T1^{HIF-1\alpha-KD}$). Scale bars: 10 µm.

© 2021 Wiley-VCH GmbH

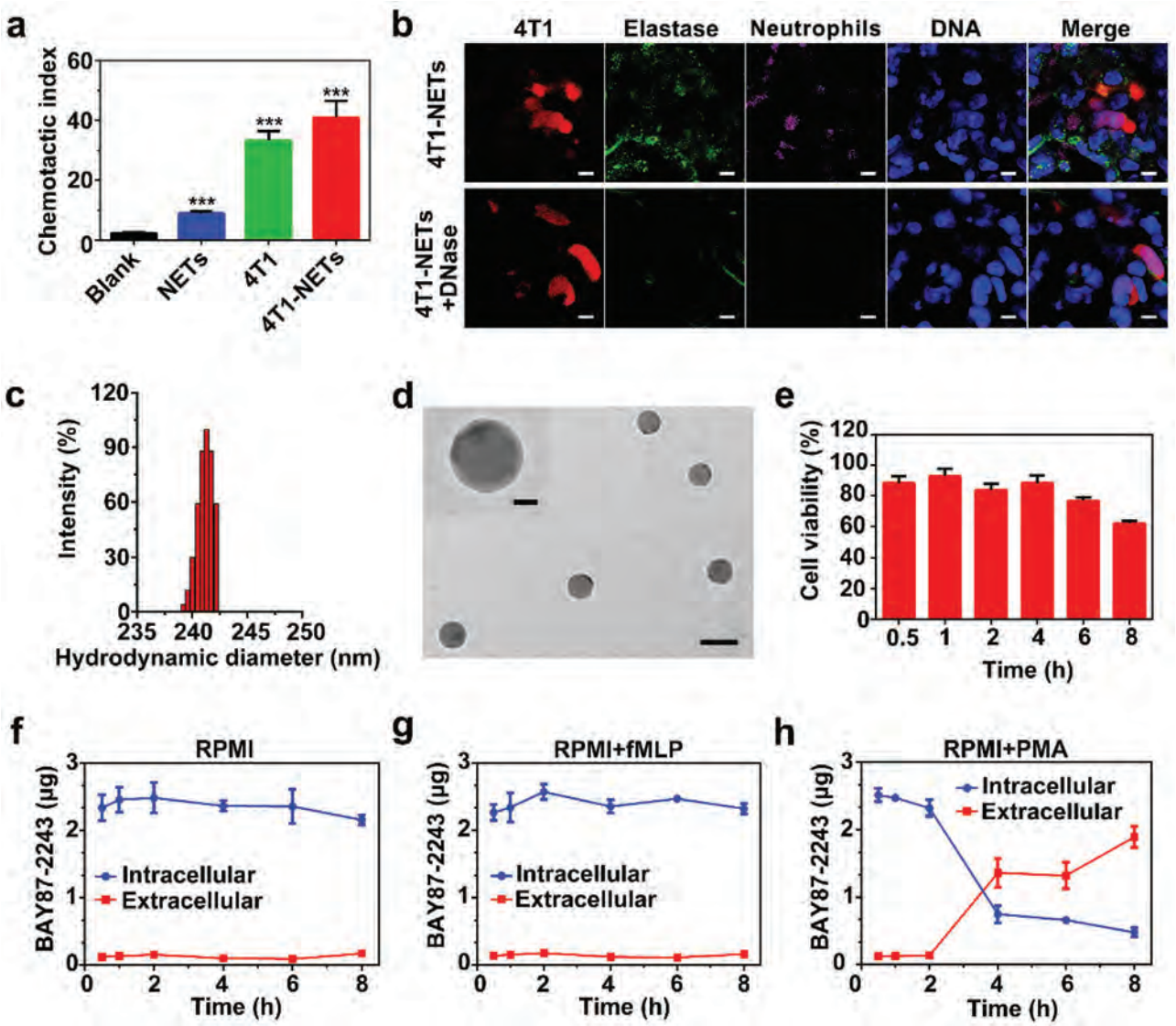

Figure 4. Preparation and characterization of BAY/NPs and CytPNEs. a) The chemotaxis activity of neutrophils toward 4T1-NET clusters as seen in transwell assays. Data are shown as mean ± SEM, from $n = 3$ independent experiments. *** $P < 0.001$ versus blank (fresh medium). b) The chemotaxis activity of neutrophils toward 4T1-NET clusters in vivo. Circulating 4T1 tumor cells (Red) were surrounded by NETs that were accompanied with neutrophil elastase (Green). The nuclei and filamentous DNA were stained by DAPI (Blue), the neutrophils were labeled with a cell membrane dye, 1,1-dioctadecyl-3,3,3,3-tetramethylindotricarbocyanine iodide (DiR, rose red). Scale bars: 5 μm. c) Histogram of particle-size distribution of BAY/NPs obtained by dynamic light scattering measurements. d) Transmission electron microscope images of BAY/NPs. Scale bars: 50 nm (inside), 200 nm (outside). e) Cell viability of CytPNEs was determined over time by the CCK-8 assay (Mean ± SEM, from $n = 3$ samples per group). f–h) Stability of CytPNEs was characterized by determining the quantity of BAY released from and retained in CytPNEs when CytPNEs were incubated in RPMI (f), RPMI with fMLP (10×10^{-9} M) (g), or RPMI with PMA (100×10^{-9} M) (h) over time (Mean ± SEM, from $n = 3$ independent experiments).

could be recruited to the 4T1-NET clusters either. The chemotaxis of CytPNEs toward 4T1-NET clusters was evaluated by transwell assay (**Figure 5**a and Figures S15 and S16, Supporting Information). We found that CytPNEs in the upper chamber could be recruited to the lower chamber containing the 4T1-NET clusters, which was similar to the chemotaxis of neutrophils. Moreover, 4T1-NET clusters possessed the strongest capacity to recruit CytPNEs compared to that of 4T1 cells or NETs alone, suggesting that NETs could assist the 4T1 cells to recruit neutrophils.[31] To investigate whether CytPNEs could be recruited to the circulating 4T1 tumor cells trapped in NETs in vivo, the DiR-labeled CytPNEs (Rose red) were administrated to the mice-bearing 4T1 lung metastasis. Similar with neutrophils without drug loading, we observed that the rose red fluorescence of CytPNEs existed nearby 4T1-NET clusters (Figure 5b), implying that CytPNEs could migrate toward NET trapped 4T1cells in vivo. Additionally, the injection of DNase decreased the level of elastase due to the NET degradation and reduced the accumulation of CytPNEs, which was in line with the transwell assay that 4T1 cells per se recruited less CytPNEs compared with 4T1-NET clusters.

© 2021 Wiley-VCH GmbH

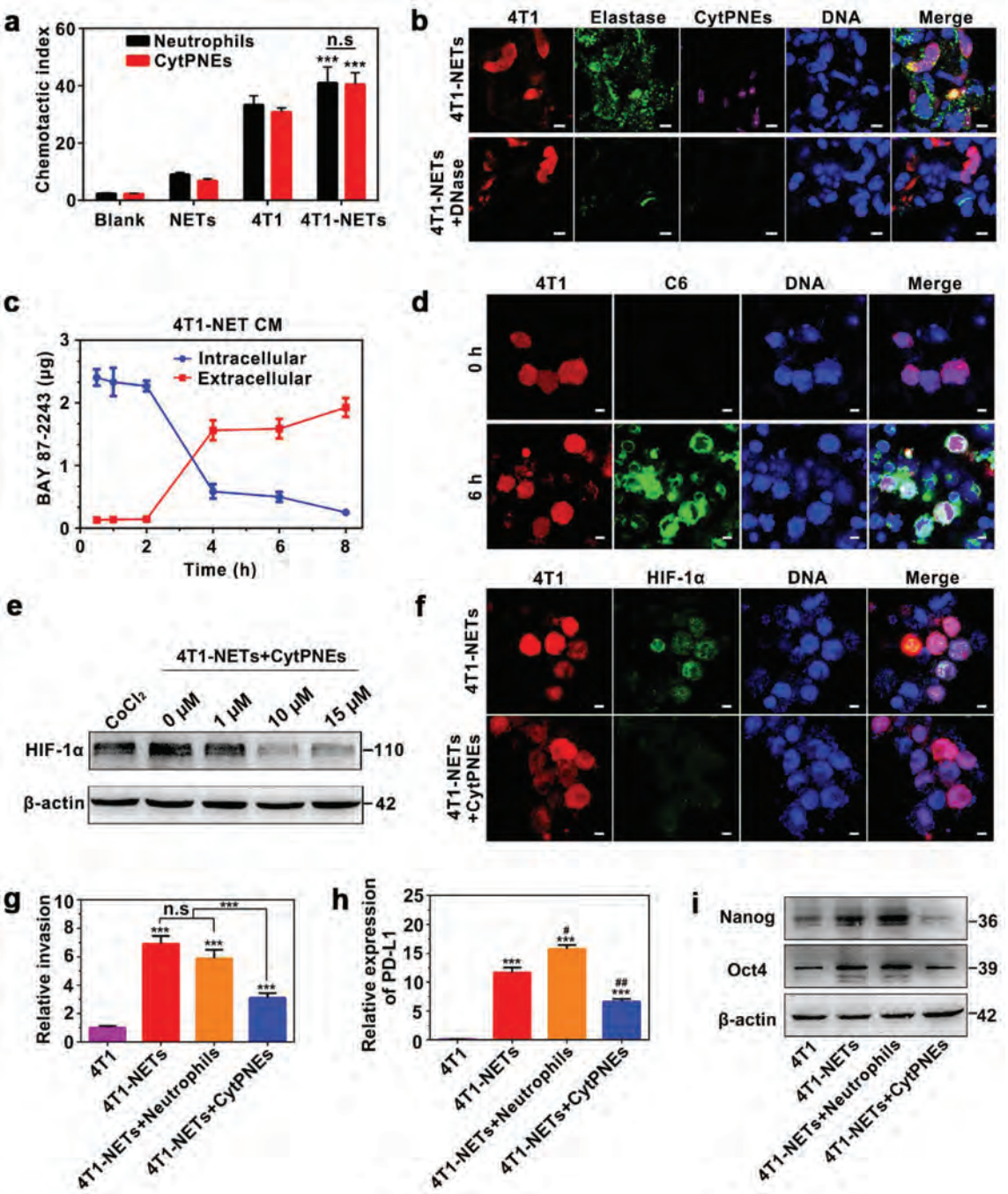

Figure 5. CytPNEs specially delivered BAY to NET trapped CTCs and interfered the HIF-1α level in CTCs. a) Chemotaxis activity of neutrophils and CytPNEs toward 4T1-NET clusters as seen using transwell assay. Data were shown as mean ± SEM, from $n = 3$ independent experiments. *** $P < 0.001$versus Blank; n.s denotes no significant difference. b) Chemotaxis activity of CytPNEs toward 4T1-NET clusters in vivo. Circulating 4T1 tumor cells (Red) were surrounded by NETs that were accompanied with neutrophil elastase (Green). The nuclei and filamentous DNA were stained by DAPI (Blue) and the CytPNEs were labeled with a cell membrane dye, 1,1-dioctadecyl-3,3,3,3-tetramethylindotricarbocyanine iodide (DiR, rose red). Scale bars: 5 μm. c) Content of BAY released from and retained in CytPNEs after incubation with CM from 4T1-NET clusters over time determined by HPLC (Mean ± SEM, from $n = 3$ independent experiments). d) C6 (Green) released from CytPNEs to 4T1(Red)-NET clusters were observed by CLSM. The nuclei were stained by Hoechst 33 342 (Blue). Scale bars: 5 μm. e) HIF-1α level in 4T1-NET clusters as detected by western blot after incubation with different concentrations of CytPNEs. f) Immunofluorescence of HIF-1α (green) in 4T1(Red)-NET clusters treated with CytPNEs at 10×10^{-6} M of BAY. The nuclei and filamentous DNA were stained by Hoechst 33 342 (Blue). Scale bars: 5 μm. g) Invasion of 4T1 cells treated with CytPNEs as seen using transwell assay (Mean ± SEM, from $n = 3$ independent experiments). $P > 0.05$. ***$P < 0.001$ versus 4T1 cells; n.s denotes no significant difference. h) Expressions of PD-L1 protein in 4T1 cells as determined by flow cytometry. Data were shown as mean ± SEM, from $n = 3$ independent experiments. *$P < 0.05$, **$P < 0.01$, ***$P < 0.001$ versus 4T1 cells. i) Expression of Nanog and Oct4 in 4T1 cells as determined by western blot. Representative gel electrophoresis bands were shown.

© 2021 Wiley-VCH GmbH

In addition, we explored the drug release from CytPNEs when they encountered NET trapped 4T1 cells rather than the mimicked inflammatory environment. Initially, we detected the extracellular and intracellular BAY content when CytPNEs were incubated with the conditioned medium (CM) of 4T1-NET clusters over time, which revealed that more than 80% BAY was released within 8 h (Figure 5c and Figure S17, Supporting Information), indicating that the 4T1-NET clusters was capable of triggering the release of loaded drug from CytPNEs. We further evaluated whether the released drug could be taken in the NET trapped 4T1 cells using CLSM (Figure 5d and Figure S18, Supporting Information). Confocal microscopy images exhibited a well colocalization of Coumarin 6 (C6, a fluorescent model drug) from the CytPNEs and 4T1 cells when incubating time increased, indicating that CytPNEs could successfully convey the drugs to the NET trapped tumor cells.

The level of HIF-1α in NET trapped 4T1 cells was detected after the treatment of CytPNEs with different concentrations for 24 h (Figure 5e). The HIF-1α accumulation in 4T1 cells with the presence of NETs was decreased in a BAY concentration-dependent manner, which was ascribed to the pharmacological inhibitory effect of BAY on HIF-1α. The inhibitory efficacy of CytPNEs on HIF-1α was further confirmed by CLSM that the green fluorescence of HIF-1α in NETs trapped 4T1 cells was obviously reduced after co-incubation with CytPNEs (Figure 5f).

Since CytPNEs strikingly suppressed the accumulation of HIF-1α in the NET trapped CTCs, we sequentially determined the expressions of downstream pro-metastasis signals of HIF-1α. We demonstrated that CytPNEs significantly suppressed the migration and invasion of 4T1 cells (Figure 5g and Figure S19, Supporting Information), as well as the expression of PD-L1 (Figure 5h and Figure S20, Supporting Information), Nanog and Oct4 in 4T1-NET clusters (Figure 5i and Figure S21, Supporting Information), compared to the 4T1-NET clusters with no treatment or with the incubation of unloaded neutrophils.

2.5. Therapeutically Targeting HIF-1α in CTCs by Living Cyto-Pharmaceuticals Significantly Prevented Lung Metastasis

To evaluate the anti-metastasis efficacy of CytPNEs in vivo, the mice bearing 4T1 lung metastasis were treated with different formulations every other day in a predetermined scheme[16] (**Figure 6**a). The number of metastatic nodules in mice treated with CytPNEs was much less than that of mice receiving BAY/NPs or free BAY, while adoptive neutrophils transfer had no obvious inhibition on the metastasis of tumors compared with saline group (Figure 6b,c). H&E- and Ki67- staining of lung sections further verified that CytPNEs effectively suppressed the colonization and metastasis formation of tumor cells at lung tissues (Figure 6b). Among all the treatments, CytPNEs exhibited the strongest inhibition rate of about 50% in the formation of lung metastases (Figure 6d), thereby leading to the longest median survival time-29 days (Figure 6e). Notably, CytPNEs exhibited the therapeutic superiority than BAY-NPs, indicating the effective delivery of BAY by neutrophils to the CTCs. All results suggested that CytPNEs effectively suppressed the colonization of circulating 4T1 cells and improved the survival of tumor-bearing mice, which can be served as potent therapeutics for the treatment of 4T1 lung metastasis.

Moreover, CytPNEs significantly restrained the proportion of PD-1$^+$ or Tim3$^+$ CD8$^+$ T cells in metastatic tumors, while BAY, BAY/NPs and neutrophils did not show similar inhibitory effects (Figure 6f and Figure S22, Supporting Information). At the same time, the expression of PD-L1 in metastatic tumors was inhibited by CytPNEs as observed in the immunofluorescent images of metastatic lung sections (Figure 6g), indicating that CytPNEs might recover the immune surveillance to some extent as a result of the effective intervention of HIF-1α in NET trapped 4T1 cells. Collectively, CytPNEs could specifically inhibit the abundance of HIF-1α in NET trapped CTCs, thereby restraining the migration, invasion, immune escape and stemness of the CTCs, finally suppressing CTC colonization and metastasis formation.

3. Discussion

CTCs, the precursor of tumor metastases, could be a potent potential target for metastasis therapy. However, challenges remain for the application of therapies that aim at CTCs due to lack of effective CTC-targeting strategy and sensitive therapeutic agents. In this study, we aim to propose a brand-new CTC- intervention strategy which combine a general therapeutic agent of HIF-1α inhibitor and an effective CTC-targeting delivery system of neutrophil cyto-pharmaceutical.

HIF-1α, the oxygen-sensitive subunit of transcription factor under hypoxia, has been considered as a critical participator in tumor metastasis,[26] but less understood in the CTCs. Here, we first verified the accumulation of HIF-1α in 4T1 cells trapped in NETs. The underlying reason that caused HIF-1α accumulation in circulating breast tumor cells could be ascribed to the high level of ROS induced by NETs. We further demonstrated that the abundance of HIF-1α in circulating 4T1 cells led to their high metastatic capacities including tissue invasion, immune escape as well as stem cell-like properties. Moreover, NETs released from neutrophils are supposed to kill microbes.[20] But recently, mounting evidences have indicated the role of NETs in promoting tumor metastasis. Together with these previous reports that NETs aided in invasion and expansion of CTCs,[10,32] our results also found that NETs assisted in breast cancer metastasis through the immune escape and the improved stem-like features. The overexpressed PD-L1 could bind to PD-1$^+$ CD8$^+$ T cells, thus protecting tumor cells from immune surveillance.[29] And the genes like Nanog and Oct4, which were predominantly regulating self-renewal and proliferation in stem cells,[33] might revoke the stemness-like ability of CTCs for facilitating metastasis.[28b,34] Of note, the overexpression of PD-L1, Nanog and Oct4 was closely associated with the level of HIF-1α, further confirming the functional role of resumed HIF-1α in breast cancer lung metastasis. It could therefore be important to develop approaches to interfere HIF-1α in CTCs for preventing metastasis.

BAY was effective in inhibiting HIF-1α accumulation,[16] however, it had been discontinued in clinical trials due to its severe gastrointestinal toxicity. Most importantly, BAY could hardly target to the pretty sparse CTCs in blood.[5] Therefore, an effective CTCs-targeting strategy is essential for renewing and expanding the application potential of BAY. Neutrophils, which are the most abundant white blood cells in peripheral blood, possess

© 2021 Wiley-VCH GmbH

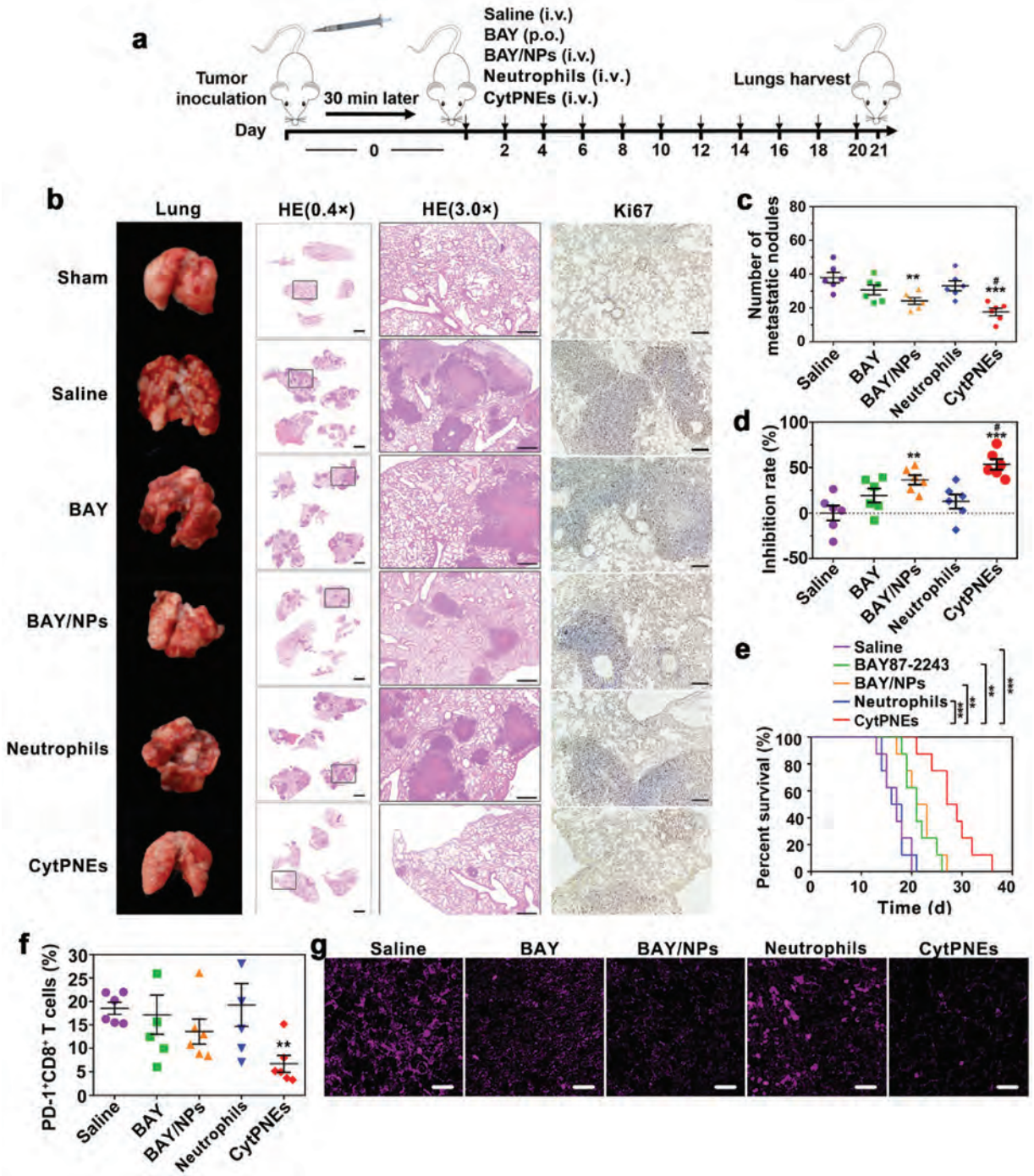

Figure 6. Therapeutically targeting HIF-1α expressing CTCs via living cyto-pharmaceuticals significantly prevented metastasis. a) Schematic illustrating the treatment of 4T1 tumor-bearing mice. After intravenous injection of 1×10^6 4T1 cells into female BALB/c mice for 30 min, the mice were treated as follows: 1) normal saline (i.v.); 2) free BAY (p.o., BAY 4 mg kg^{-1}); 3) BAY/NPs (i.v., BAY 1 mg kg^{-1}); 4) native neutrophils (i.v., 5×10^6 cells/mouse); 5) CytPNEs (i.v., 5×10^6 cells/mouse, equivalent to a dose of 1 mg kg^{-1} of BAY). Mice were treated every other day from day 1 to day 21, and sacrificed at day 22. Lung tissues were harvested for further evaluation. b) Typical images of lung tissues, H&E stained and Ki67 stained lung sections from 4T1 tumor-bearing mice after treatment. The normal mice treated with saline served as sham group. Scale bars: 2000 µm (H&E 0.4×), 500 µm (H&E 3.0×) and 150 µm (Ki67). c) Numbers of visually detected metastatic nodules in lungs from each group (Mean ± SEM; $n = 6$ samples per group). $^{**}P < 0.01$, $^{***}P < 0.001$ versus saline, $^{\#}P < 0.05$ versus BAY/NP. d) Inhibition rates of lung metastasis of 4T1-bearing mice receiving different treatments, compared to the saline treatment (Mean ± SEM; $n = 6$ samples per group). $^{**}P < 0.01$, $^{***}P < 0.001$ versus saline, $^{\#}P < 0.05$ versus BAY/NP. e) Survival percentage of mice receiving different treatments ($n = 8$ per group). $^{**}P < 0.01$, $^{***}P < 0.001$. f) The proportion of PD-1$^+$ CD8$^+$ T cells in lung tissues harvested from mice with different treatments (Mean ± SEM; $n = 6$ samples per group). $^{**}P < 0.01$ versus saline. g) Immunofluorescence of PD-L1 (Rose red) in lung sections harvested from mice with different treatments. Scale bars: 10 µm.

© 2021 Wiley-VCH GmbH

the natural chemotaxis toward inflammatory signals.[30] Previously, we have utilized neutrophils as cytotoxicity drug carriers for chemotherapy after treatment by invasive surgery,[17a] local radiotherapy[17b] or photothermal therapy[17c] due to the enlarged inflammatory signal. Here, we found that the 4T1-NET clusters recruited more neutrophils compared with NETs or circulating 4T1 cells alone, which was probably due to the increasing formation of inflammatory environment with secreted chemokines such as CXCL1/CXCL2, IL-8 and so on.[35] Since the native chemotaxis ability of neutrophils to the CTC-NET clusters, we designed a living neutrophil cyto-pharmaceutical loaded with BAY-nanoparticles. Our in vitro and in vivo studies demonstrated that the cyto-pharmaceuticals could be recruited to the 4T1-NET clusters and released their encapsulated drugs, leading to the effective down-regulation of HIF-1α in 4T1 cells and its downstream effectors, and thereby prolonging the life-span of metastatic breast cancer-bearing mice. These results indicated that the recovered HIF-1α in circulating 4T1 cells was an attractive target to suppress metastasis, which could be specially targeted by the living cyto-pharmaceuticals. In addition, the decreased amount of BAY in the gastrointestinal tract might improve its in vivo safety. However, to thoroughly investigate the reliability of recovered HIF-1α in CTCs as a therapeutic target, clinical samples are urgently needed. Additionally, the anti-metastatic efficacy of ROS scavengers or compounds to block the formation of NETs deserves a further investigation.

4. Conclusions

In conclusion, our data provide a new perspective for understanding the role of NETs in HIF-1α accumulation in circulating breast tumor cancer cells, and expand the role of HIF-1α abundance in tumor metastasis cascades which can be served as a potent therapeutic target for the treatment of breast cancer metastasis. Meanwhile, we have successfully prepared the living neutrophil cyto-pharmaceuticals to specifically deliver the HIF-1α inhibitor to the circulating breast tumor cancer cells, which can achieve the potent anti-metastasis effect and put forward the strategy of targeted intervention of CTCs as a meaningful treatment for tumor metastasis.

5. Experimental Section

Cell Lines: Murine mammary adenocarcinoma cells (4T1 cell line) obtained from Shanghai Cell Bank, Chinese Academy of Sciences, were cultured in RPMI-1640 medium (HyClone, Thermo Fisher Scientific) with 10% fetal bovine serum (Gibco, Thermo Fisher Scientific). Human umbilical vein endothelial cells (HUVECs) obtained from American Type Culture Collection, were cultured in high glucose DMEM medium (HyClone, Thermo Fisher Scientific) with 10% fetal bovine serum (Gibco, Thermo Fisher Scientific).

Generation of $4T1^{HIF-1\alpha-KD}$ cell line. 4T1 cells with stable expression of Cas9 were established by lentiviral infection. 293 T cells were used to product lentivirus according to the manufacturer's instructions (Lenti-Pac HIV Expression Packaging Kit, GeneCopoeia). Then 4T1 cells were infected with 5 μg mL^{-1} polybrene and lentivirus for 24 h. After that, 4T1-cas9 stably expressed cells were selected by blasticidin (2 μg mL^{-1}) for 7 days. Next, single-guide RNAs (sgRNA) including control and HIF-1α sgRNA were cloned into the pCRISPR-LvSG03 vector, whose sequences were listed as following: control sgRNA 5-GGCTTCGCGCCGTAGTCTTA-3; HIF-1α sgRNA 5- TTTCTTCTCGTTCTCGCCGC-3. Then, the 4T1-cas9 cells were infected with the sgRNA. After infection, the sgRNA infected 4T1-cas9 cells were cultured in the media containing 2 μg mL^{-1} puromycin to select for sgRNA.

4T1-mCherry cells were obtained by infecting with mCherry lentiviral vector.

Mice: Female BALB/c mice (18–22 g) were purchased from the Comparative Medicine Center of Yangzhou University. All animals were treated according to the guidelines for the care and use of laboratory animals approved by the Animal Science Ethics Committee of China Pharmaceutical University.

Materials: The antibodies for PD-L1 (CD274 Monoclonal Antibody, 17-5982-80; thermo), HIF-1α (ab179483; abcam), PHD1 (ab113077; abcam), PHD2 (ab133630; abcam), PHD3 (ab18471; abcam), neutrophil elastase (ab68672; abcam), PD-1 coupled with FITC (135 213; BioLegend), CD8 coupled with PE (12-008782; eBioscience) and Lymphocyte antigen 6G/Gr-1 coupled with Alexa Fluor 488 (108 417; BioLegend) were commercially available. Secondary antibody used in immunofluorescence assays was Alexa Fluor 488 donkey anti-rabbit IgG(H+L) (A21206; Invitrogen). The Ac-DEX[36] was synthesized by Liu's group, and ditetradecyl lysylglutamate (TA_2-Glu-Lys, TA_2GL) and BAY 87–2243 were synthesized by the group. Other reagents such as DNase (10 104 159 001; Sigma), N-formyl-L-methionyl-L-leucyl-L-phenylalanine tripeptide (fMLP) (47 729; Sigma), Phorbol 12-myristate 13-acetate (PMA) (P8139; Sigma), $CoCl_2$ (V900021; Sigma), DiR (KGMP0026; KeyGEN BioTECH), DiO (C1038; Beyotime Biotechnology), Hoechst 33 342 (C1022 Beyotime Biotechnology) were purchased from the indicated suppliers.

In Vivo Characterization of NET Trapped CTCs: Female BALB/c mice were injected with mCherry expressing 4T1 cells (1×10^6 cells per mouse) into their tail vein, and the mice were sacrificed 24 h later. The lungs were harvested, followed by washing with saline and fixing with 4% paraformaldehyde at 4°C for 2 h. Subsequently, 15% and 30% sucrose were used to dehydrate overnight. After dehydration, the tissues were embedded with OCT and cut into 15 μm sections. The slices were immersed in PBS buffer for 10 min. Then, the OCT embedding agent around the tissues was removed and the liquid on the surface of the slices was dried. The sections were blocked with 5% BSA at 37°C for 30 min and then incubated with neutrophil elastase and CD31 antibodies at 4°C for overnight. The sections were washed with PBST (0.5% Tween-20 in PBS) 3 times and incubated with fluorescent antibodies at 37°C for 1 h, washed with PBST three times, and stained with DAPI. The sections were observed using a confocal laser scanning microscope (CLSM) (LSM880, Carl Zeiss Jena).

HIF-1α Level in NET Trapped CTCs In Vivo: The lung tissues were obtained and cut into 15 μm sections as described above. The slices were immersed in PBS buffer for 10 min, the OCT embedding agent around the tissues was removed, and the liquid on the surface of the slices was dried. The sections were blocked with 5% BSA at 37°C for 30 min and then incubated with HIF-1α and CD31 antibodies at 4°C for overnight. The sections were washed with PBST (0.5% Tween-20 in PBS) 3 times and incubated with fluorescent antibodies at 37°C for 1 h, washed with PBST three times, and stained with DAPI. The sections were observed using a CLSM (LSM880, Carl Zeiss Jena).

Preparation and Characterization of 4T1-NET Clusters In Vitro: Neutrophils were isolated from bone marrow of healthy BALB/c mice by a Percoll gradient centrifugation as previously reported.[17a] Then, 1×10^6 neutrophils were plated in 6-well culture plates and incubated at 37°C for 30 min. Then, PMA was added (1×10^{-6} M final concentration) into the medium to induce the formation of NETs. The medium containing PMA was discarded, and NETs were washed with PBS carefully. Afterward, 2×10^5 4T1 cells were added and cultured for another 16 h at 37°C to form the 4T1-NET clusters.

The 4T1-NET clusters were immobilized by 4% paraformaldehyde (PFA) for 10 min. After carefully washing three times with PBS, the clusters were blocked with 5% BSA at 37°C for 30 min and incubated with the neutrophil elastase antibody overnight at 4°C. Next day, the clusters were washed with PBS three times, followed by incubation with the second, fluorescent antibody at 37°C for 1 h. After washing with PBS for three times, nuclei were stained with Hoechst 33 342 at room temperature for 15 min. Then

© 2021 Wiley-VCH GmbH

the clusters were washed with PBS for three times and identified using a CLSM (LSM880, Carl Zeiss Jena).

Scanning electron microscopy (SEM) was used to identify the clusters. 4T1-NET clusters were seeded on sterile slides and incubated for 16 h at 37°C. Then, the medium was carefully discarded. The 4T1-NET clusters were fixed with 2.5% glutaraldehyde overnight at 4°C and washed 3 times with distilled water for about 5 min each. Dehydration was carried out according to an ethanol concentration gradient of 30%, 50%, 70%, 80%, 90%, 100%, 100%, and 100% (v:v), and the slides were air-dried at room temperature. The samples were sprayed with gold and the SEM images were obtained using a JEOL JSM-7600F instrument at 10.0 kV.

HIF-1α Level in 4T1-NET Clusters: Identification of the clusters by immunofluorescence microscopy was carried out as follows. The clusters were fixed with 4% paraformaldehyde for 10 min, followed by 0.5% Triton X-100 to perforate cell membranes at room temperature. After careful washing with PBS 3 times, the samples were blocked at 37°C for 30 min with 5% BSA. The clusters were incubated with primary antibodies to HIF-1α, neutrophil elastase or H3Cit overnight at 4°C. After careful washing with PBS, clusters were incubated with the fluorescent secondary antibody Alexa Fluor 488 or 647 in a 37°C incubator for 1 h. The clusters were washed twice with PBS and stained with Hoechst 33 342 for 15 min at room temperature. After washing twice more, samples were observed using a CLSM (LSM880, Carl Zeiss Jena).

Western blot was also used to analyze the HIF-1α level in 4T1-NET clusters. Briefly, total protein of the clusters was extracted with SDS cell lysis buffer (Beyotime, China) containing 1% proteinase inhibitor cocktail (CW-Bio, China) according to the manufacturer's instructions. Proteins were separated using 10% SDS-polyacrylamide gel electrophoresis, followed by electro-transfer to polyvinylidene fluoride (PVDF) membranes. HIF-1α and β-actin primary rabbit antibodies were employed. Horseradish peroxidase-conjugated goat anti-rabbit/mouse IgG (Boster, Wuhan, China) was used as the secondary antibody. Immunoreactive bands were visualized with Tanon 5200 Multi Chemiluminescence Imaging System and analyzed with Image J.

Resumed HIF-1α in NET Trapped CTCs: 4T1 cells were initially incubated under hypoxia for 24 h followed by another incubation under normoxia for 2 h. Subsequently, the PMA (1×10^{-6} M)-triggered NETs were utilized to trap 4T1 cells at normoxia condition for the formation of CTC-NET clusters. Western blot was used to analyze the HIF-1α level as detailed above.

ROS Levels in 4T1-NET Clusters: 4T1-NET clusters were plated in 12-well tissue culture plates and allowed to incubate for 16 h at 37°C in RPMI without or with 1 mg mL^{-1} DNase. Untreated 4T1 cells in RPMI served as controls. Cells were digested with 0.25% trypsin and suspended in 300 µL RPMI, followed by incubation with 2,7-dichlorofuorescin diacetate (10×10^{-6} M final concentration) at 37°C for 30 min. After thrice washing with ice cold PBS, cells were analyzed with a n Attune NxT Acoustic focusing flow cytometer (Thermo Fisher Scientific).

Cellular Migration and Invasion Assay: For migration assay, 6-well chambers with 3-µm pore polyester membranes were used. 2×10^5 4T1 cells, 4T1-NET clusters, $4T1^{HIF1\alpha-KD}$-NET clusters and 4T1-NET clusters incubated with DNase (1 mg mL^{-1}) or BAY (10×10^{-6} M) were added into the upper chamber. After 24 h of incubation, 12 random fields of the cells that had migrated across the transwell membrane to the lower chamber were photographed and counted to calculate the relative migration using Image J. Relative migration mean the average cell areas in visual fields of each group normalized to that of the 4T1 group.

For invasion assays, 6-well chambers with 8-µm polyester membranes were used with the inserts precoated with 1×10^4 HUVECs that had been allowed to form monolayers with a trans epithelial electric resistance (TEER) greater than 250 Ω cm^{-2} (Millicell Resistor Instrument). Then, 2×10^5 each of 4T1 cells, 4T1-NET clusters, $4T1^{HIF1\alpha-KD}$-NET clusters and 4T1-NET clusters incubated with DNase (1 mg mL^{-1}) or BAY (10×10^{-6} M) were added into the upper chamber. After 24 h of incubation, 12 random fields of the invaded cells in the bottom of culture plates were photographed and counted to calculate the relative invasion using Image J. Relative invasion mean the average cell areas in visual field of each group normalized to that of 4T1 group.

PD-L1 Expression: For the detection of PD-L1, 4T1-NET clusters and $4T1^{HIF-1\alpha-KD}$-NET clusters were plated in 12-well tissue culture plates and incubated without or with BAY (10×10^{-6} M). 4T1 cells and $4T1^{HIF-1\alpha-KD}$ cells were used as controls. After incubation for 16 h, cells and clusters were digested with 0.25% trypsin and suspended in 300 µL RPMI containing allophycocyanin (APC) -conjugated PD-L1 antibody for further 30 min incubation at 37°C. After washing twice with PBS stained cells were analyzed by Attune NxT Acoustic focusing flow cytometer (Thermo Fisher Scientific).

Nanog and Oct4 Expression: Western blot was used to analyze the Nanog and Oct4 expression as detailed above. The following primary antibodies were employed: anti-Nanog, anti-Oct4 and anti-β-actin. Horseradish peroxidase-conjugated goat anti-rabbit/mouse IgG was used as the secondary antibody.

Tumor Metastasis Promoting Activity of Resumed HIF-1α: Female BALB/c mice were injected with 4T1 cells or $4T1^{HIF-1\alpha-KD}$ cells (1×10^6 cells per mouse) into the tail vein; some of the mice receiving 4T1 cells were also injected with DNase (2.5 mg kg^{-1}) intramuscularly at the same time. There were six mice in each group and mice were sacrificed after 3 weeks. The lung tissues were collected and fixed with 4% PFA. The number of metastatic nodules on the tissue surface was counted. Then the fixed lung tissues were embedded in paraffin, sectioned and stained with HE or Ki67 antibody. The sections were observed using a Nikon Eclipse Ts2R inverted fluorescence microscope.

To investigate the ratios of $PD\text{-}1^+$ or $Tim3^+$ $CD8^+$ T cells in the lung tissues, the lung tissues harvested from mice that had received 4T1 cells, 4T1 cells and DNase, and $4T1^{HIF-1\alpha-KD}$ cells were digested with 1mg mL^{-1} collagenase IV (Sigma, USA), followed by 40% and 70% (v:v) Percoll density gradient centrifugation. The obtained cell suspensions were stained with anti-CD8 and anti-PD-1 fluorescent antibodies at 4°C for 1 h. Finally, cells were subjected to flow cytometry analysis using a FACSCalibur flow cytometer.

For the detection of PD-L1, the lung tissues harvested from mice that had received 4T1 cells, 4T1 cells and DNase, and $4T1^{HIF-1\alpha-KD}$ cells were washed with saline and fixed with 4% paraformaldehyde at 4°C for 2 h. Subsequently, 15% and 30% sucrose were used to dehydrate overnight. After dehydration, the tissues were embedded with OCT and cut into 15 µm sections. The sections were blocked with 3% BSA at 37°C for 30 min and then incubated with APC-conjugated PD-L1 antibody at 37°C for 1h. After washed with PBST for three times, they were stained with DAPI and observed using a CLSM (LSM880, Carl Zeiss Jena).

Preparation and Characterization of BAY/NPs: The preparation of BAY/NPs was performed by a modified oil-in-water (o/w) nanoemulsion solvent evaporation method. In brief, Ac-DEX (25 mg) and BAY (5 mg) were dissolved in 0.25 mL of ethyl acetate and added to 0.75 mL of polyvinyl alcohol (PVA 0486) solution (1% v/v in dd-H_2O). The mixture was emulsified by ultrasonication for 30 s in an ice bath using a probe sonicator (10 s pulses intercalated with 2 s intervals, 30% amplitude). The resulting solution was added to 10 mL of polyvinyl alcohol solution (1% v/v in dd-H_2O, pH 8.5 adjusted with 1×10^{-3} M NaOH). Then, the mixture was evaporated to remove organic solvent under continuous stirring for 4 h. Nanoparticles were isolated by centrifugation at 13 780 *g* for 6 min and washed with dd-H_2O (pH 8.5) for three cycles. Next, the positive lipid TA_2GL (4 mg) was dissolved in 0.25 mL of dd–H_2O (pH 8.5) and mixed with the nanoparticles. After vortex, bath sonication (5 min) and centrifugation at 13780 *g* for 6 min, the final BAY/NPs were obtained by redispersion in dd–H_2O (pH 8.5). Average particle size and zeta potential were determined using a Particle/Protein Size and Zeta Potential Analyzer (Brookhaven, Nanobrook Omni).

For morphology analysis, BAY/NPs were dropped onto a copper mesh with carbon film, and then negatively stained with 0.1% sodium phosphotungstate solution. The samples were analyzed by a transmission electron microscopy (Hitachi HT-7700, Japan) at 100 KV.

Preparation of CytPNEs: Neutrophils were isolated from bone marrow as described above. neutrophils (1×10^5 cells mL^{-1}) were incubated with BAY/NPs (60 µg mL^{-1} final concentration of BAY) for 20 min at 37°C. Then, the CytPNEs were obtained after washing with PBS for 3 times. For the preparation of neutrophils loaded with C6/NPs (C6/NPs-loaded

© 2021 Wiley-VCH GmbH

neutrophils), neutrophils (1×10^5 cells mL^{-1}) were incubated with C6/NPs at a C6 concentration of 40 ng mL^{-1} at 37 °C for 20 min. The subsequent procedure was similar to that of CytPNEs.

BAY Determination: For BAY/NPs, the nanoparticles were diluted in acetonitrile. After vortex and bath sonication for 5 min, the solution was centrifuged at 13 780 *g* for 10 min. The BAY in the supernatant (20 µL) was quantified using HPLC (Shimadzu LC2010A). The mobile phase was a mixture of acetonitrile and water (50/50, v/v). A InertSustain C18 column (4.6 mm × 250 mm × 5 µm, GL Sciences Inc, Japan) was employed for analysis at a flow rate of 1 mL min^{-1}. The detection wavelength was set at 250 nm and the column temperature at 40°C.

For CytPNEs, cells were firstly lysed with SDS cell lysis buffer (Beyotime, China). The cell lysate (50 µL) was mixed with 200 µL of acetonitrile, vortexed for 5 min and centrifuged at 13780 *g* for 10 min. The supernatant (20 µL) was injected into the HPLC system for quantification.

Cell Viability of CytPNEs: Freshly prepared CytPNEs were plated into 96-well plates (5×10^5 cells per well) and incubated at 37°C in a 5% CO_2 incubator. 10 µL of CCK-8 (Yeasen Biotech Co., Ltd, China) was added into the corresponding wells at 0.5, 1, 2, 4, 6, and 8 h, followed by another 2 h incubation. The absorbance at 450 nm was measured. Six replicate wells were set in each group. Fresh medium was used as a negative control. Native neutrophils at 0 h were set as the 100% activity standard.

In Vitro Stability of CytPNEs: The in vitro stability of CytPNEs was evaluated under different conditions, including the normal physiological condition, during the process of chemotaxis, at the site of inflammation. fMLP and PMA were applied to simulate the chemotactic cytokines in the blood circulation and at the site of inflammation, respectively. In brief, 8×10^5 CytPNEs were seeded in 24-well plates, and then incubated with the RPMI and RPMI containing fMLP (10×10^{-9} M) and PMA (100×10^{-9} M) for different periods (0.5, 1, 2, 4, 6, and 8 h). The amounts of BAY in the CytPNEs and released in the supernatant medium were determined using HPLC.

In Vivo Inhibitory Effects of CytPNEs on Lung Metastasis: To construct the breast cancer lung metastasis model, 4T1 cells (1×10^6 cells per mouse) suspended in saline were injected into the tail vein of female BALB/c mice. Then the mice were randomly divided into 5 groups (n = 6 per group). 30 min later, the following treatments were performed: 1) normal saline (i.v.); 2) free BAY (p.o., BAY 4 mg kg^{-1}); 3) BAY/NPs (i.v., BAY 1 mg kg^{-1}); 4) native neutrophils (i.v., 5×10^6 cells per mouse); 5) CytPNEs (i.v., 5×10^6 cells per mouse, equivalent to a dose of 1 mg kg^{-1} of BAY). Mice were administered every other day for totally 11 injections and sacrificed three weeks later.

For metastatic measurement, the lung tissues were harvested and washed with PBS. Tissues were then fixed with 4% paraformaldehyde and photographed. The number of metastatic nodules on the surface of the tissues was counted for statistical analysis. The fixed lung tissues were embedded in paraffin, sliced and stained with HE or Ki67 antibody, followed by observation using a Nikon Eclipse Ts2R inverted fluorescence microscope. The inhibition rate (%) = $(N_{\text{saline}} - N_{\text{formulation}})/N_{\text{saline}} \times 100\%$. N_{saline} indicates the mean number of metastatic nodules of lungs from 4T1-bearing mice treated with saline, while $N_{\text{formulation}}$ indicates the mean number of metastatic nodules of lungs from 4T1-bearing mice treated with other formulations.

To investigate the ratios of PD-1^+ $CD8^+$ T cells in the lung tissues, the lung tissues harvested from tumor-bearing mice after different treatments were handled as mentioned above and analyzed by FACSCalibur flow cytometry.

For the detection of PD-L1, the lung tissues harvested from tumor-bearing mice after different treatments were analyzed as described above and observed using CLSM (LSM880, Carl Zeiss Jena).

For the survival study, mice were treated as described above (n = 8 per group). The mice were kept for the study of long-term survival.

Recruitment of Neutrophils and CytPNEs by NET Trapped CTCs: To investigate the recruitment of neutrophils and CytPNEs in vitro, 6-well chambers with 3-µm pore polyester membranes were used. 4T1-NET clusters were seeded on the bottom of 6-well tissue culture plates and incubated for 16 h. Freshly prepared neutrophils or CytPNEs (1×10^6, cells were stained with a cell membrane dye, 3,3′-dioctadecyloxacarbocyanine perchlorate (DiO)) were added to the chamber. After another 24 h of incubation, the recruited cells across the transwell to the culture plates were quantified by measuring green fluorescence intensity at 12 random fields. 4T1 cells and NETs served as controls, respectively, and fresh RPMI was used as a negative control. Chemotaxis index was calculated according to the following formula: Chemotaxis index = average fluorescence intensity per field/total fluorescence intensity per field × 100%. The total fluorescence intensity was measured by directly plating 1×10^6 neutrophils or CytPNEs onto the bottom of the transwell membrane.

For investigation of the recruitment of neutrophils and CytPNEs in vivo, female BALB/c mice were intravenously injected with 4T1-mCherry cell suspension (1×10^6 cells). 24 h later, freshly prepared neutrophils or CytPNEs (5×10^6, cells were stained with DiR) were injected per mouse. After 2 h, the mice were sacrificed and dissected. The lung tissues were harvested and followed by cryotomy (CM3050S, Leica) and observation using CLSM (LSM880, Carl Zeiss Jena).

Drug Delivery from CytPNEs to NET Trapped CTCs: To confirm the drug release from CytPNEs when they reached the 4T1-CTC clusters, the CM of 4T1-CTC clusters was collected. 8×10^5 CytPNEs were seeded in 24-well plates, and then incubated with the CM of 4T1-CTC clusters for different periods (0.5, 1, 2, 4, 6, and 8 h). The amounts of BAY in the CytPNEs released into the supernatant medium were determined using HPLC.

In addition, to explore the delivery of C6 from CytPNEs to the clusters, C6/NPs-loaded CytPNEs were directly incubated with the 4T1-NET clusters in vitro for different periods (0, 1, 2, 4, and 6 h) followed by observation using CLSM (LSM880, Carl Zeiss Jena).

In Vitro Effect of CytPNEs on HIF-1α Expression and Downstream Proteins: 4T1-NET clusters were prepared in six-well plates, and different amounts of fresh CytPNEs were added to the clusters with the final BAY concentrations of 0, 1, 10 and 15×10^{-6} M, respectively. After incubation at 37°C for 24 h, the culture medium was carefully removed, and the clusters were washed twice with PBS. The SDS cell lysate containing protease inhibitor was added to each well. The cell extracts were transferred to 1.5 mL EP tubes and fully lysed for 30 min. To ensure that the total amount of protein is equal between each group, the same volume but complementary number of cells are added to the cell lysate of each group to ensure that the total number of neutrophils and neutrophils added to the 4T1-NET complex in each group is equal. Western blot analysis was performed as described above. The following primary antibodies were employed: anti-HIF-1α, anti-Nanog, anti-Oct4 and anti-β-actin.

To confirm the HIF-1α level in 4T1-NET clusters after the treatment with CytPNEs, the HIF-1α level in clusters was identified by immunofluorescence. The clusters were fixed with 4% paraformaldehyde for 10 min, followed by 0.5% Triton X-100 to perforate cell membranes at room temperature. After careful washing with PBS 3 times, the samples were blocked at 37°C for 30 min with 5% BSA. The clusters were incubated with primary antibodies to HIF-1α overnight at 4°C. After careful washing with PBS, the clusters were incubated with fluorescent secondary antibody Alexa Fluor 488 donkey anti-rabbit IgG (H+L) in a 37°C incubator for 1 h. The clusters were washed twice with PBS and stained with Hoechst 33 342 for 15 min at room temperature. After washing twice more, samples were observed using a CLSM (LSM880, Carl Zeiss Jena).

Statistical Analysis: Statistical analyses were performed using GraphPad Prism 8.0. All plots show Mean ± SEM from at least three independent experiments. The Student's *t*-test was applied for comparisons between two groups, one-way ANOVA test was used for comparisons of multiple groups, and a log-rank (Mantel–Cox) test was used to analyze the statistical significance of difference for survival analysis. Statistical significance was set at $^*P < 0.05$, $^{**}P < 0.01$, and $^{***}P < 0.001$.

Supporting Information

Supporting Information is available from the Wiley Online Library or from the author.

 © 2021 Wiley-VCH GmbH

Acknowledgements

Y.Z. and C.W. contributed equally to this work. The authors thank the Public Platform of the State Key Laboratory of Natural Medicines for assistance with the pathological-section imaging. This work was supported by the National Natural Science Foundation of China (81930099, 82130102, 81773664, 82073785), the Natural Science Foundation of Jiangsu Province (BK20212011), "Double First-Class" University project (CPU2018GY47, CPU2018GF10), 111 Project from the Ministry of Education of China and the State Administration of Foreign Expert Affairs of China (No. 111-2-07, B17047), and the Open Project of State Key Laboratory of Natural Medicines (No. SKLNMZZ202017).

Conflict of Interest

The authors declare no conflict of interest.

Data Availability Statement

The data that support the findings of this study are available from the corresponding author upon reasonable request.

Keywords

circulating tumor cells, HIF-1α, neutrophil cyto-pharmaceuticals, neutrophil extracellular traps, tumor metastasis

Received: August 24, 2021
Revised: November 12, 2021
Published online:

[1] a) D. X. Nguyen, P. D. Bos, J. Massague, *Nat. Rev. Cancer* **2009**, *9*, 274; b) J. Massague, A. C. Obenauf, *Nature* **2016**, *529*, 298.
[2] Z. Diamantopoulou, F. Castro-Giner, N. Aceto, *J. Exp. Med.* **2020**, *217*, 20200356.
[3] J. Yao, J. Feng, X. Gao, D. Wei, T. Kang, Q. Zhu, T. Jiang, X. Wei, J. Chen, *Biomaterials* **2017**, *113*, 1.
[4] M. Xu, K. Hu, Y. Liu, Y. Huang, S. Liu, Y. Chen, D. Wang, S. Zhou, Q. Zhang, N. Mei, H. Lu, F. Li, X. Gao, J. Chen, *Nat. Commun.* **2021**, *12*, 3187.
[5] J. M. Lang, B. P. Casavant, D. J. Beebe, *Sci. Transl. Med.* **2012**, *4*, 141ps13.
[6] F. Castro-Giner, N. Aceto, *Genome Med.* **2020**, *12*, 31.
[7] G. Bergers, S. M. Fendt, *Nature Rev. Cancer* **2021**, *21*, 162.
[8] L. Schito, G. L. Semenza, *Trends Cancer* **2016**, *2*, 758.
[9] G. Kallergi, H. Markomanolaki, V. Giannoukaraki, M. A. Papadaki, A. Strati, E. S. Lianidou, V. Georgoulias, D. Mavroudis, S. Agelaki, *Breast Cancer Res.* **2009**, *11*, R84.
[10] J. Park, R. W. Wysocki, Z. Amoozgar, L. Maiorino, M. R. Fein, J. Jorns, A. F. Schott, Y. Kinugasa-Katayama, Y. Lee, N. H. Won, E. S. Nakasone, S. A. Hearn, V. Kuttner, J. Qiu, A. S. Almeida, N. Perurena, K. Kessenbrock, M. S. Goldberg, M. Egeblad, *Sci. Transl. Med.* **2016**, *8*, 361ra138.
[11] L. Erpenbeck, M. P. Schon, *Oncogene* **2017**, *36*, 2483.
[12] A. S. Savchenko, J. I. Borissoff, M. Kimberly, S. F. Meyer, De, G. M., E. Luise, B. Alexander, W. Yanming, D. D. Wagner, *Blood* **2014**, *123*, 141.
[13] S. K. Jorch, P. Kubes, *Nat. Med.* **2017**, *23*, 279.
[14] G. L. Semenza, *Blood* **2009**, *114*, 2015.
[15] D. Gerald, E. Berra, Y. M. Frapart, D. A. Chan, A. J. Giaccia, D. Mansuy, J. Pouyssegur, M. Yaniv, F. Mechta-Grigoriou, *Cell* **2004**, *118*, 781.
[16] P. Ellinghaus, I. Heisler, K. Unterschemmann, M. Haerter, H. Beck, S. Greschat, A. Ehrmann, H. Summer, I. Flamme, F. Oehme, K. Thierauch, M. Michels, H. Hess-Stumpp, K. Ziegelbauer, *Cancer Med.* **2013**, *2*, 611.
[17] a) J. Xue, Z. Zhao, L. Zhang, L. Xue, S. Shen, Y. Wen, Z. Wei, L. Wang, L. Kong, H. Sun, Q. Ping, R. Mo, C. Zhang, *Nat. Nanotechnol.* **2017**, *12*, 692; b) C. Ju, Y. Wen, L. Zhang, Q. Wang, L. Xue, J. Shen, C. Zhang, *Small* **2019**, *15*, 1804191; c) L. Zhang, Y. Zhang, Y. Xue, Y. Wu, Q. Wang, L. Xue, Z. Su, C. Zhang, *Adv. Mater.* **2019**, *31*, 1805936.
[18] T. Mohanty, J. Sjogren, F. Kahn, A. H. Abu-Humaidan, N. Fisker, K. Assing, M. Morgelin, A. A. Bengtsson, N. Borregaard, O. E. Sorensen, *Blood* **2015**, *126*, 2128.
[19] J. Cools-Lartigue, J. Spicer, B. McDonald, S. Gowing, S. Chow, B. Giannias, F. Bourdeau, P. Kubes, L. Ferri, *J. Clin. Invest.* **2013**, *123*, 3446.
[20] V. Brinkmann, U. Reichard, C. Goosmann, B. Fauler, Y. Uhlemann, D. S. Weiss, Y. Weinrauch, A. Zychlinsky, *Science* **2004**, *303*, 1532.
[21] J. P. Piret, D. Mottet, M. Raes, C. Michiels, *Ann. N. Y. Acad. Sci.* **2002**, *973*, 443.
[22] A. C. Epstein, J. M. Gleadle, L. A. McNeill, K. S. Hewitson, J. O'Rourke, D. R. Mole, M. Mukherji, E. Metzen, M. I. Wilson, A. Dhanda, Y. M. Tian, N. Masson, D. L. Hamilton, P. Jaakkola, R. Barstead, J. Hodgkin, P. H. Maxwell, C. W. Pugh, C. J. Schofield, P. J. Ratcliffe, *Cell* **2001**, *107*, 43.
[23] E. Piskounova, M. Agathocleous, M. M. Murphy, Z. Hu, S. E. Huddlestun, Z. Zhao, A. M. Leitch, T. M. Johnson, R. J. DeBerardinis, S. J. Morrison, *Nature* **2015**, *527*, 186.
[24] D. Stojkov, P. Amini, K. Oberson, C. Sokollik, A. Duppenthaler, H. U. Simon, S. Yousefi, *J. Cell Biol.* **2017**, *216*, 4073.
[25] N. W. Eyrich, C. R. Potts, M. H. Robinson, V. Maximov, A. M. Kenney, *Mol. Cell. Biol.* **2019**, *39*, 00268.
[26] C. C. Wong, D. M. Gilkes, H. Zhang, J. Chen, H. Wei, P. Chaturvedi, S. I. Fraley, C. M. Wong, U. S. Khoo, I. O. Ng, D. Wirtz, G. L. Semenza, *Proc. Natl. Acad. Sci. USA* **2011**, *108*, 16369.
[27] L.-N. Qi, B.-D. Xiang, F.-X. Wu, J.-Z. Ye, J.-H. Zhong, Y.-Y. Wang, Y.-Y. Chen, Z.-S. Chen, L. Ma, J. Chen, W.-F. Gong, Z.-G. Han, Y. Lu, J.-J. Shang, L.-Q. Li, *Cancer Res.* **2018**, *78*, 4731.
[28] a) M. Mohme, S. Riethdorf, K. Pantel, *Nat. Rev. Clin. Oncol.* **2017**, *14*, 155; b) S. Gkountela, F. Castro-Giner, B. M. Szczerba, M. Vetter, J. Landin, R. Scherrer, I. Krol, M. C. Scheidmann, C. Beisel, C. U. Stirnimann, C. Kurzeder, V. Heinzelmann-Schwarz, C. Rochlitz, W. P. Weber, N. Aceto, *Cell* **2019**, *176*, 98.
[29] E. A. Mittendorf, A. V. Philips, F. Meric-Bernstam, N. Qiao, Y. Wu, S. Harrington, X. Su, Y. Wang, A. M. Gonzalez-Angulo, A. Akcakanat, A. Chawla, M. Curran, P. Hwu, P. Sharma, J. K. Litton, J. J. Molldrem, G. Alatrash, *Cancer Immunol. Res.* **2014**, *2*, 361.
[30] E. Kolaczkowska, P. Kubes, *Nat. Rev. Immunol.* **2013**, *13*, 159.
[31] A. S. Savchenko, J. I. Borissoff, K. Martinod, S. F. De Meyer, M. Gallant, L. Erpenbeck, A. Brill, Y. Wang, D. D. Wagner, *Blood* **2014**, *123*, 141.
[32] E. Kolaczkowska, C. N. Jenne, B. G. Surewaard, A. Thanabalasuriar, W. Y. Lee, M. J. Sanz, K. Mowen, G. Opdenakker, P. Kubes, *Nat. Commun.* **2015**, *6*, 6673.
[33] D. L. van den Berg, T. Snoek, N. P. Mullin, A. Yates, K. Bezstarosti, J. Demmers, I. Chambers, R. A. Poot, *Cell Stem Cell* **2010**, *6*, 369.
[34] T. Liu, H. Xu, M. Huang, W. Ma, D. Saxena, R. A. Lustig, M. Alonso-Basanta, Z. Zhang, D. M. O'Rourke, L. Zhang, Y. Gong, G. D. Kao, J. F. Dorsey, Y. Fan, *Cancer Res.* **2018**, *78*, 6632.
[35] S. Acharyya, T. Oskarsson, S. Vanharanta, S. Malladi, J. Kim, P. G. Morris, K. Manova-Todorova, M. Leversha, N. Hogg, V. E. Seshan, L. Norton, E. Brogi, J. Massague, *Cell* **2012**, *150*, 165.
[36] D. Liu, H. Zhang, E. Makila, J. Fan, B. Herranz-Blanco, C. F. Wang, R. Rosa, A. J. Ribeiro, J. Salonen, J. Hirvonen, H. A. Santos, *Biomaterials* **2015**, *39*, 249.

© 2021 Wiley-VCH GmbH